Received: 6 February 2021 | Revised: 27 April 2021 | Accepted: 7 September 2021

DOI: 10.1002/mgg3.1815

Molecular Genetics & Genomic Medicine Open Access WILEY

ORIGINAL ARTICLE

Clinical and molecular characterization of five Chinese patients with autosomal recessive osteopetrosis

Huanhuan Liang[1] | **Niu Li**[2,3] | **Ru-en Yao**[2,3] | **Tingting Yu**[2,3] | **Lixia Ding**[1] | **Jing Chen**[1] | **Jian Wang**[2,3]

[1]Key Laboratory of Pediatric Hematology and Oncology, Ministry of Health, Department of Hematology and Oncology, Shanghai Children's Medical Center, Shanghai Jiao Tong University School of Medicine, Shanghai, China

[2]Department of Medical Genetics and Molecular Diagnostic Laboratory, Shanghai Children's Medical Center, Shanghai Jiao Tong University School of Medicine, Shanghai, China

[3]Shanghai Key Laboratory of Clinical Molecular Diagnostics for Pediatrics, Shanghai, China

Correspondence
Jian Wang, Shanghai Children's Medical Center, Shanghai Jiao Tong University School of Medicine, 1678 Dongfang Road, Shanghai 200127, P.R. China.
Email: labwangjian@shsmu.edu.cn

Funding information
This research was sponsored by grants from the Program of Shanghai Academic/Technology Research Leader (19XD1422600 and 2018BR28), Project of Shanghai Municipal Science and Technology Commission (20dz2260900), and Shuguang Program supported by the Shanghai Education Development Foundation and Shanghai Municipal Education Commission (18SG14).

Abstract

Background: Osteopetrosis is characterized by increased bone density and bone marrow cavity stenosis due to a decrease in the number of osteoclasts or the dysfunction of their differentiation and absorption properties usually caused by biallelic variants of the *TCIRG1* and *CLCN7* genes.

Methods: In this study, we describe five Chinese children who presented with anemia, thrombocytopenia, hepatosplenomegaly, repeated infections, and increased bone density. Whole-exome sequencing identified five compound heterozygous variants of the *CLCN7* and *TCIRG1* genes in these patients.

Results: Patient 1 had a novel variant c.1555C>T (p.L519F) and a previously reported pathogenic variant c.2299C>T (p.R767W) in *CLCN7*. Patient 2 harbored a novel missense variant (c.1025T>C; p.L342P) and a novel splicing variant (c.286-9G>A) in *CLCN7*. Patients 3A and 3B from one family displayed the same compound heterozygous *TCIRG1* variant, including a novel frameshift variant (c.1370del; p.T457Tfs*71) and a novel splicing variant (c.1554+2T>C). In Patient 4, two novel variants were identified in the *TCIRG1* gene: c.676G>T; p.E226* and c.1191del; p.P398Sfs*5. Patient 5 harbored two known pathogenic variants, c.909C>A (p.Y303*) and c.2008C>T (p.R670*), in *TCIRG1*. Analysis of the products obtained from the reverse transcription-polymerase chain reaction revealed that the c.286-9G>A variant in *CLCN7* of patient 2 leads to intron 3 retention, resulting in the formation of a premature termination codon (p.E95Vfs*8). These five patients were eventually diagnosed with autosomal recessive osteopetrosis, and the three children with *TCIRG1* variants received hematopoietic stem cell transplantation.

Conclusions: Our results expand the spectrum of variation of genes related to osteopetrosis and deepen the understanding of the relationship between the genotype and clinical characteristics of osteopetrosis.

KEYWORDS

autosomal recessive osteopetrosis, cDNA sequencing, *CLCN7*, novel variant, *TCIRG1*

1 | INTRODUCTION

Osteopetrosis is a genetic heterogeneous rare disease characterized by abnormal bone metabolism. Its pathogenesis stems from the dysfunction of differentiation and/or absorption of osteoclasts, which results in skeletal dysplasia, such as increased bone density, brittleness, and medullary cavity stenosis (Ajmal et al., 2017; Deng et al., 2016; Pangrazio et al., 2014; Shamriz et al., 2017). Three major clinical forms of osteopetrosis have been described, namely autosomal recessive osteopetrosis (ARO) (OMIM #259700), intermediate autosomal osteopetrosis (IAO) (OMIM #259710), and autosomal dominant osteopetrosis (ADO) (OMIM #166600), which differ in hereditary characteristics, age of onset and clinical presentation (Besbas et al., 2009; Sobacchi et al., 2013; Zeng et al., 2016). ARO, known as infantile malignant osteopetrosis, is the most fatal type of osteopetrosis (Bonapace et al., 2014). Patients with ARO often develop symptoms in infancy or childhood, and in addition to abnormalities in the skeletal system, they often present with pathological changes in other systems, such as hepatosplenomegaly, pancytopenia, hydrocephalus, optic atrophy, repeated infections, and others (Kuroyanagi et al., 2014; Stark et al., 2013). ADO is more likely to be benign, and it is usually reported in adolescents or adults (Moore et al., 2017). The clinical symptoms of ADO may include fracture due to minor trauma, osteomyelitis, and hematological and neural defects of varying severity, but no systemic symptoms have been described (Moore et al., 2017). Although patients with ADO display increased bone density, their life expectancy is usually normal even without any treatment (Sobacchi et al., 2013). The clinical manifestations and severity of IAO are between those of ARO and ADO.

ARO is a genetically and clinically heterogeneous disorder with an incidence of 1/250 000 in the general population (Bliznetz et al., 2009). Two subtypes of ARO have been described, including the osteoclast-rich-dysfunction ARO caused by variants of *TCIRG1* (OMIM 604592), *CLCN7* (OMIM 602727), *OSTM1* (OMIM 607649), *SNX10* (OMIM 614780), and *PLEKHM1* (OMIM 611466), and the osteoclast-poor ARO caused by variants of *TNFSF11* (OMIM 602642) and *TNFRSF11A* (OMIM 603499) (Anderson et al., 2015). Of these, biallelic variants of *TCIRG1* (~50%), *CLCN7* (13–16%), and *OSTM1* (2–6%) account for most patients with ARO (Pangrazio, Frattini, et al., 2012). The *TCIRG1* gene, located on human chromosome 11q13.2, contains 22 exons, which encode the a3 subunit of V-ATPase composed of 830 amino acids. V-ATPase is a proton pump, and its main function is to pump hydrogen ions into the secretory lysosome. When hydrogen ions are pumped out of the osteoclast, they acidify the cortical environment between the osteoclast and bone tissue, promoting bone reabsorption and regulating bone formation and development (Pangrazio, Caldana, et al., 2012). In 1999, it has been shown that osteoclast V-ATPase of the oc/oc *Tcirg1*-deficient mice exhibited serious defects, and it was initially confirmed proposed that the *TCIRG1* mutation may be one of the main causes of osteoclast dysfunction in humans (Li et al., 1999). The *CLCN7* gene, located on human chromosome 16p13.3, contains 25 exons, which encode chloride channel protein 7 (CIC-7) of 803 amino acids. CLCN7 is a member of the voltage-gated chloride channel protein family that mediates the exchange of chloride ions against protons, maintaining the acidic environment for bone resorption (Sobacchi et al., 2013). CLCN7 plays a synergistic role when hydrogen ions are transported outside of the cell by TCIRG1 (Yu et al., 2014).

Hematopoietic stem cell transplantation (HSCT) is currently the only effective therapy for osteopetrosis, but its efficacy depends on the patient's genotype (Anderson et al., 2015). It has been reported that individuals with *OSTM1* gene abnormality and some *CLCN7* gene mutations accompanied by neurodegeneration do not show improvement after HSCT (Sobacchi et al., 2013). Further, HSCT does not affect the course of osteopetrosis in individuals with mutations in the *TNFSF11* gene, which encodes osteoclast differentiation and activation factor, and does not reverse renal tubular acidosis and kidney injury caused by *CAII* gene mutations (Herebian et al., 2017; Sobacchi et al., 2013). Therefore, identification of the causative variants in each case of osteopetrosis is pivotal for the decision whether HSCT can be performed.

In this study, we performed whole-exome sequencing of five children with suspected osteopetrosis. We detected seven novel variants in two genes, *TCIRG1* and *CLCN7*, and analyzed the pathogenicity of these variants.

2 | MATERIALS AND METHODS

2.1 | Ethical compliance

Patients in this study were recruited from the Shanghai Children's Medical Center (SCMC). Informed consent was obtained from parents of all patients. The Ethics Committee of the SCMC approved this study (approval #SCMCIRB-K2016013).

2.2 | Study subjects

All five patients were born to non-consanguineous healthy parents. Patient 1 was a four-year and seven-month-old boy, who was transferred to the hematology clinic of the

SCMC due to osteomyelitis and strabismus. The initial laboratory findings revealed mild anemia (hemoglobin: 97 g/L), granulocytosis (5.9×10^9/L), monocytopenia (0.8×10^9/L), and elevated reticulocytes (4.6%). The white blood cell (WBC) count and platelet count were normal. Imaging examination showed a significant increase in bone density, and the vertebral endplate showed a typical "sandwich vertebrae" appearance (Figure 1a).

Patient 2 was a one-year and ten-month-old girl, with a height of 83 cm (−0.4 SD) and a weight of 11.2 kg (−0.1 SD). She was presented to the infectious disease clinic at our hospital with a cold and a cough. The patient was normally delivered at full term with a birth weight of 3 300 g. When she was half a month old, she was found to have pancytopenia, strabismus, nystagmus, and hypotonia, and displayed no significant improvement after treatment with nutritional neuropharmaceuticals. The motor development milestones of this patient were severely delayed; she could not raise her head, could not sit and stand up without support, and could not talk. The laboratory findings showed mild anemia (hemoglobin, 97 g/L), elevated reticulocytes (4.2%), and elevated lactate dehydrogenase (1 562 U/L). The WBC, monocyte and platelet counts, IgG, serum calcium, and alkaline phosphatase levels were normal. Palpation of the abdomen showed hepatosplenomegaly. We observed that her bone density increased, part of the medullary cavity disappeared, and the vertebral endplate thickened, resulting in the "sandwich vertebrae" appearance, according to the chest X-ray examination (Figure 1b).

Patient 3A was the first daughter of the family. She was delivered at full term with a birth weight of 3900 g. She had thrombocytopenia (65×10^9/L) at the age of 20 days, and improved after 2 months of oral prednisone treatment. At 13 months of age, her height was 66 cm (>−3.0 SD), her weight was 7.7 kg (−1.9 SD), and she was again taken to the hematology clinic for thrombocytopenia. Her motor development milestones were normal. Clinical laboratory investigations revealed moderate anemia (hemoglobin, 64 g/L), leukocytosis (38.7×10^9/L), thrombocytopenia (20×10^9/L), mononucleosis (5.1×10^9/L), elevated reticulocytes (7.5%), elevated lactate dehydrogenase

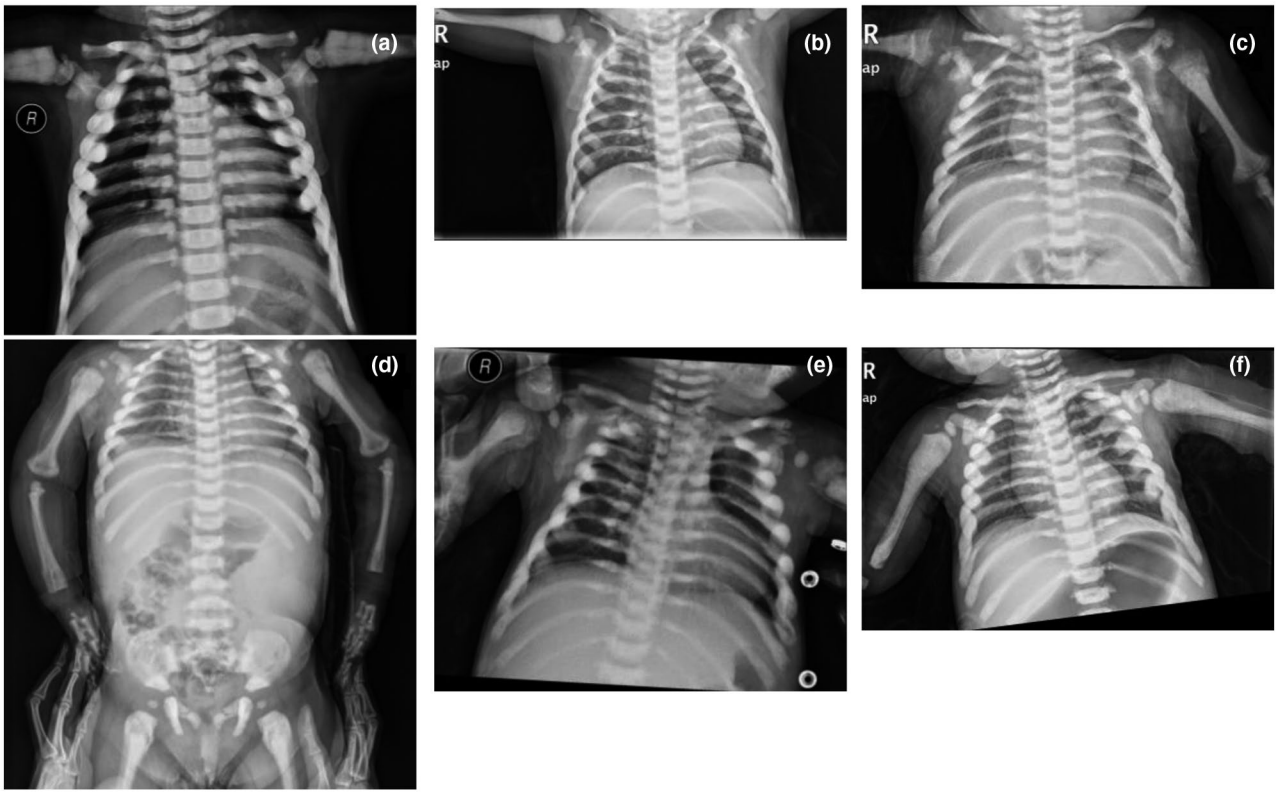

FIGURE 1 Patient X-rays. Patient 1 (a) A significant increase in bone density was observed, and the vertebral endplate showed the typical "sandwich vertebrae" appearance. Patient 2 (b) The results showed that bone density increased, part of the medullary cavity disappeared, the vertebral endplate thickened, and the "sandwich vertebrae" appearance was observed. Patient 3A (c) A significant increase in bone density was evident. Patient 3B (d) Diffusely increased bone density was confirmed, and the long bones with obliterated marrow cavity showed the typical "bone in bone" appearance. Patient 4 (e) A diffuse increase in bone density was observed, and the marrow cavity of the long bones disappeared, showing the "bone in bone" appearance. Patient 5 (f) A generalized increase in bone density was evident, the marrow cavity of the long bones disappeared, and the vertebral endplate appeared thickened, having the "sandwich vertebrae" appearance

(2 924 U/L), increased alkaline phosphatase (785 IU/L), and normal serum calcium levels. Abdominal palpation showed hepatosplenomegaly. Chest radiography showed a significant increase in bone density (Figure 1c). She was diagnosed with juvenile-myelomonocytic-leukemia (JMML), did not receive any medical care, and died soon after. Patient 3B was an 8-month-old girl, 65 cm tall (−1.9 SD) with normal weight (7.9 kg, −0.6 SD). She presented with thrombocytopenia (70×10^9/L) and bleeding in the limbs and abdominal skin. She was the second baby of the family and 2 years younger than Patient 3A, with a normal birth weight of 3700 g. When she was 2 months old, her limbs and abdominal skin displayed repeated occurrences of bleeding, and she was found to have thrombocytopenia and hepatosplenomegaly. Her development milestones were normal. Admission laboratory examinations revealed moderate anemia (hemoglobin, 64 g/L), leukocytosis (21.75×10^9/L), thrombocytopenia (55×10^9/L), mononucleosis (1.62×10^9/L), elevated reticulocytes (6.9%), elevated lactate dehydrogenase (1088 U/L), and increased alkaline phosphatase (500 IU/L), whereas serum calcium levels were normal. Abdominal palpation showed no improvement in hepatosplenomegaly. X-ray examination revealed diffusely increased bone density, and the long bones with obliterated marrow cavities showed the typical "bone in bone" appearance at the time of admission (Figure 1d).

Patient 4, a 13-month-old boy with a height of 67 cm (>−3.0 SD) and a weight of 8.8 kg (−1.2 SD), was sent to the hematology clinic due to persistent high fever and hepatosplenomegaly. When he was 3 months old, he presented with moderate anemia (hemoglobin: 75 g/L) and thrombocytopenia (33×10^9/L). He presented with strabismus and nystagmus at the age of 7 months and hepatosplenomegaly at the age of 8 months. His development milestones were delayed, and he needed support to sit. Laboratory results indicated moderate anemia (hemoglobin: 88 g/L), leukocytosis (16.48×10^9/L), mononucleosis (2.01×10^9/L), elevated reticulocytes (10.3%), elevated lactate dehydrogenase (2 219 U/L), increased alkaline phosphatase (610 IU/L), and decreased serum calcium levels (1.63 mmol/L), with a normal platelet count. Abdominal palpation showed no improvement in the hepatosplenomegaly symptoms. X-rays showed a diffuse increase in bone density, and the marrow cavity of the long bones disappeared with the "bone in bone" appearance (Figure 1e).

Patient 5, a 1-year-old boy (height: 71 cm, −2.0 SD; weight: 8 kg, −2.0 SD), was referred to the hematology clinic for persistent high fever. He was the first child of the family and was born at term via normal delivery with a birth weight of 3 150 g. He presented with a recurrent upper respiratory tract infection after birth, and was found to display growth retardation at a local hospital at the age of 2 months. His motor development milestones were delayed, and he could sit by himself, but could not stand up without support. The laboratory results showed moderate anemia (hemoglobin: 77 g/L), leukocytosis (19.87×10^9/L), thrombocytopenia (59×10^9/L), mononucleosis (2.1×10^9/L), elevated reticulocytes (4.0%), a compromised immune system (IgG: 1.55g/L), elevated lactate dehydrogenase (2377 U/L), increased alkaline phosphatase (616 IU/L), and normal serum calcium levels. Palpation of the abdomen revealed hepatosplenomegaly. X-ray examination revealed a generalized increase in bone density, the marrow cavity of the long bones disappeared, and the vertebral endplate was thickened with the "sandwich vertebrae"' appearance (Figure 1f). He received treatment only against the infections.

Clinical and laboratory data of the five patients are presented in Table 1.

2.3 | DNA sample preparation

Genomic DNA was extracted from peripheral blood samples obtained from patients and parents using a QIAamp DNA Blood Mini Kit (Qiagen, Hilden, Germany) according to the manufacturer's instructions. The DNA sample was quantified using a Qubit dsDNA BR Assay Kit (Life Technologies).

2.4 | Whole-exome sequencing and data analysis

Approximately 3 μg of genomic DNA from each sample was processed through shearing to 150–200 bp pieces using a Covaris M220 Focused-ultrasonicator (Covaris). An adaptor-ligated library was constructed using a Paired-end Sequencing Library prep Kit (Agilent Technologies). The design of the capture library was performed and enriched using an Agilent SureSelect XT Human All Exon V6 Kit (Agilent Technologies). Clusters were then generated using isothermal bridge amplification with an IllUmina cBot station, and the products were sequenced on an Illumina HiSeq2500 System (Illumina).

Base calling and sequence read quality assessments were evaluated using Illumina Sequence Control Software v4.0.4 with real-time analysis (Illumina, Inc.). Sequencing reads were aligned to the reference human genome (GRCh37.3, SNP135) using NextGENe® (SoftGenetics LLC). All single-nucleotide variants and insertion-deletions were saved in a VCF format file and uploaded to the Ingenuity® Variant Analysis platform (Ingenuity System, Redwood City, CA, USA) for bioinformatics analysis and interpretation.

TABLE 1 Summary of clinical findings of the patients

Patients	Patient 1	Patient 2	Patient 3A	Patient 3B	Patient 4	Patient5
General information						
Sex	Male	Female	Female	Female	Male	Male
Age at diagnosis	4 years 7 months	1 year 10 months	1 year 1 month	8 months	1 year 1 month	1 year
Birth weight(g)	Unknown	3 300	3 900	3 700	3 650	3 150
Current height (cm)	Unknown	83 (−0.4SD)	66 (>−3SD)	65 (−1.9SD)	67 (>−3SD)	71 (−2.0SD)
Current weight (kg)	Unknown	11.2 (−0.1SD)	7.7 (−1.9SD)	7.9 (−0.6SD)	8.8 (−1.2SD)	8.0 (−2.0SD)
Results of blood chemistry						
RBC ($3.70–5.80 \times 10^{12}$/L)	3.66	3.85	2.13	2.17	3.36	2.86
WBC ($4.0–15.0 \times 10^{9}$/L)	9.43	8.95	38.70	21.75	16.48	19.87
Hemoglobin (110–160g/L)	97	97	64	64	88	77
Platelets ($100–550 \times 10^{9}$/L)	204	194	20	55	104	59
Monocyte ($0.1–0.6 \times 10^{9}$/L)	0.80	0.47	5.10	1.62	2.01	2.10
Reticulocyte (0.5–0.15%)	4.6	4.2	7.5	6.9	10.3	4
LDH (313–618 U/L)	Unknown	1562	2924	1088	2219	2377
ALP (<500 IU/L)	Unknown	203	785	500	610	616
Calcium (2.23–2.80 mmol/L)	Unknown	2.40	2.30	2.29	1.63	2.45
Ig G (4.7–12.3g/L)	8.12	5.89	Unknown	Unknown	Unknown	4.15
Other findings						
Hepatosplenomegaly	Unknown	Yes	Yes	Yes	Yes	Yes
Increased bone density	Yes	Yes	Yes	Yes	Yes	Yes
Motor development milestones	Unknown	Severely delayed	Normal	Normal	Delayed	Delayed
Optic nerve symptoms/age at onset	Unknown	Strabismus, nystagmus/15 days	NO	NO	Strabismus, nystagmus/7 months	NO

Abbreviations: ALP, alkaline phosphatase; Ig G, immunoglobulin GLDH, lactate dehydrogenase; RBC, red blood cell; SD, standard deviation; WBC, white blood cells.

2.5 | Sanger sequencing

Sanger sequencing was performed to confirm the results identified in the patients using whole-exome sequencing. The primers (Table S1) for CLCN7 (NM_001287.6) and *TCIRG1* (NM_006019.4) were designed by UCSC ExonPrimer online software (http://genome.ucsc.edu/index.html). The target sequences were amplified using polymerase chain reaction (PCR) and examined by electrophoresis in a 1% agarose gel. The products were purified using a QIAquik Gel Extraction Kit (Qiagen), and the sequencing was performed on an ABI Prism 3730XL Genetic Analyzer (Applied Biosystems; Thermo Fisher). The sequence data obtained were analyzed with Mutation Surveyor® software, version 4.0.4 (SoftGenetics).

2.6 | Reverse transcription-polymerase chain reaction (RT-PCR)

To determine the splicing of the *CLCN7* c.286-9G>A variant, total RNA from peripheral blood samples of the patient and parents was extracted using a total RNA mini kit (TianGen). Then, cDNA was obtained using a reverse transcription system kit (Qiagen). The following primers were used for PCR amplification of a 290-bp fragment of the wild-type cDNA: forward primer 5′-GAGTCGGACATATGAGCAGC-3′ located in exon 2 and reverse primer 5′-CCAGGTTTTCCACCACGATG-3′ located in exon 5. The products were examined using electrophoresis in a 1% agarose gel and cloned into the pMD19-T vector (Takara Biotechnology (Dalian) Co, Ltd.), thereafter 40 clones were selected and sequenced. *GAPDH* was used as control to assess RNA quality, and a 99-bp region of the *GAPDH* gene was amplified using PCR with the following primers: forward, 5′-GGACCTGACCTGCCGTCTAG-3′ and reverse, 5′-TAGCCCAGGATGCCCTTGAG-3′.

2.7 | Pathogenicity predictions of the validated variants

The potential pathogenicity of the validated missense variant was predicted using PolyPhen-2 (http://genetics.bwh.harvard.edu/pph2/), PROVEAN (http://provean.jcvi.org/protein_batch_submit.php?species=human), MutationAssessor (http://mutationassessor.org/r3/), and Mutation taster (http://www.mutationtaster.org/ChrPos.html). The UCSC genome browser (http://genome.ucsc.edu/) was used to roughly analyze the conservation of the mutated amino acid.

3 | RESULTS

3.1 | Identification of *TCIRG1* and *CLCN7* variants

Whole-exome sequencing was used to screen for the causal variants in the five patients. The candidate variants were initially filtered after excluding benign variants predicted by SIFT (http://sift.Jcvi.org/) and PolyPhen-2 software, low-confidence variants, and high-frequency variants with an allele frequency >1% in the gnomAD database. Clinical symptoms of anemia, hepatosplenomegaly, and increased bone density were used as the filtering indicator to analyze the above-screened candidate variants. Finally, variants in *TCIRG1* and *CLCN7* were found that most likely caused the above-described manifestations in the patients studied.

Compound heterozygous variants were identified in the *CLCN7* gene (NM_001287.6) in Patient 1. One variant, c.1555C>T, inherited from the father, was a novel missense variant in exon 17 that leads to an amino acid conversion (p.L519F). Another variant, c.2299C>T (p.R767W), which was inherited from the mother, has been reported previously (Figure 2a,b) (Deng et al., 2016; Zhang et al., 2009). Patient 2 exhibited compound heterozygous variants c.286-9G>A and c.1025T>C in *CLCN7*. The novel splicing variant c.286-9G>A was inherited from the father, and the novel missense variant c.1025T>C in exon 12, which leads to an amino acid conversion (p.L342P), was inherited from the mother (Figure 2a,c). Compound heterozygous variants c.1370del and c.1554+2T>C in the *TCIRG1* gene (NM_006019.4) were identified in Patient 3B. The novel variant c.1370del, inherited from the father, leads to a premature stop codon (p.T457Tfs*71). The novel splicing variant c.1554+2T>C, inherited from the mother, is located in intron 13 (Figure 2a,d). The same compound heterozygous variants were detected in the cryopreserved blood sample of Patient 3A. Patient 4 harbored a compound heterozygous variant in *TCIRG1*, including one novel nonsense variant c.676G>T (p.E226*) in exon 5 and a novel deletion of a single base (c.1191del) in exon 11, which results in the formation of a premature stop codon (p.P398Sfs*5). The c.676G>T (p.E226*) variant was inherited from the father and the c.1191del (p.P398Sfs*5) variant was inherited from the mother (Figure 2a,e). Compound heterozygous variants, c.909C>A (p.Y303*) and c.2008C>T (p.R670*), were identified in *TCIRG1* in Patient 5. Both variants have been reported previously (Yu et al., 2014). Further, the father carried the c.909C>A (p.Y303*) variant, and the mother carried the c.2008C>T (p.R670*) variant (Figure 2a,f).

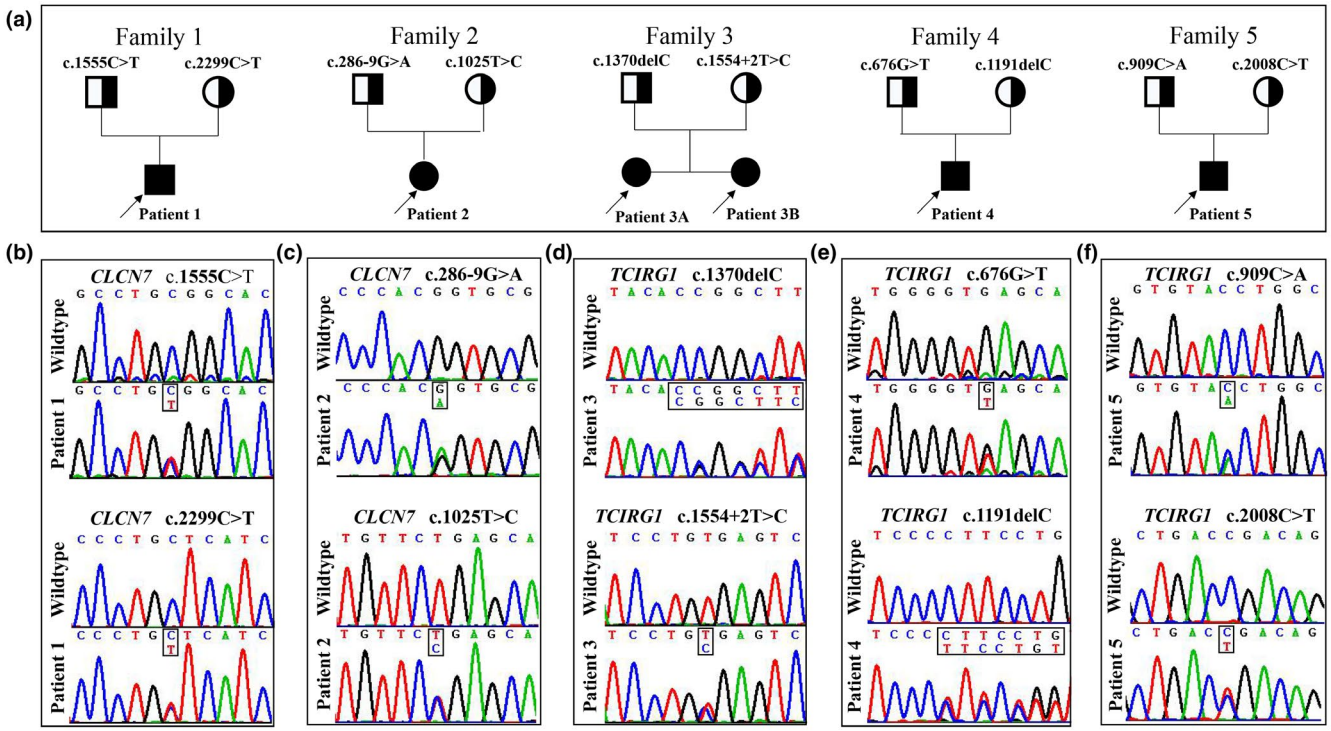

FIGURE 2 Family pedigrees and genetic sequencing findings. (a) The pedigrees of all patients. (b–f) Variants in the *CLCN7* and *TCIRG1* genes identified by WES were verified using Sanger sequencing. (b) We identified compound heterozygous variants c.1555C>T (p.L519F) and c.2299C>T (p.R767W) in the *CLCN7* gene in Patient 1. (c) Patient 2 displayed compound heterozygous variants c.286-9G>A and c.1025T>C in the *CLCN7* gene. (d) Compound heterozygous variants c.1370del and c.1554+2T>C were identified in the *TCIRG1* gene in Patients 3A and 3B. (e) Patient 4 harbored a compound heterozygous variant in the *TCIRG1* gene (c.676G>T; p.E226* in exon 5 and c.1191del in exon 11). (f) Compound heterozygous variants c.909C>A (p.Y303*) and c.2008C>T (p.R670*) were identified in the *TCIRG1* gene in Patient 5. All patients inherited the variants from their parents, respectively

3.2 | Pathogenicity predictions of the c.1025T>C (p.L342P) and c.1555C>T (p.L519F) variants in the *CLCN7* gene

The *CLCN7* p.L342P and p.L519F variants, observed in Patients 2 and 1, respectively, occur in the voltage-gated chloride channel domain, which is highly conserved in multiple species (Figure 3a). In addition, the leucines at positions 342 and 519 in the CLCN7 protein are highly conserved (Figure 3b,c). We next evaluated the pathogenicity of the c.1025T>C (p.L342P) and c.1555C>T (p.L519F) variants using four types of prediction software. The prediction results for c.1025T>C (p.L342P) are listed in Table 2. The PolyPhen-2 score was 1, indicating that this variant was possibly damaging. The PROVEAN score was −11.48, showing that this variant was deleterious. The Mutation Assessor score was 3.13, which implied that this variant exerted a medium effect on the function of the CLCN7 protein. The MutationTaster score was 1, indicating that this variant was disease-causing.

The prediction results for c.1555C>T (p.L519F) are also displayed in Table 2. The PolyPhen-2 score was 1, which indicated that this variant was probably damaging. The PROVEAN score was −11.59, suggesting that this variant was deleterious. The Mutation Assessor score was 2.36, which showed that this variant exerted a medium effect on the function of the CLCN7 protein. The MutationTaster score was 1, indicating that this variant was disease-causing. These findings indicate that both variants in the *CLCN7* gene were pathogenic.

3.3 | Transcriptional analysis of the *CLCN7* c.286-9G>A variant

In order to determine whether the c.286-9G>A variant affects *CLCN7* mRNA splicing, total RNA from the patient and her parents was extracted to detect cDNA sequence alterations between exons 2 and 5. Gel electrophoresis displayed two bands of different sizes. The smaller product (lower band), approximately 290 bp, was assumed to be the wild-type *CLCN7*, which was present in the patient's mother (Figure 3d). The larger product (upper band) was observed in the patient and her father who carried the c.286-9G>A variant (Figure 3d). TA clone analysis of the RT-PCR products revealed that the wide-type product

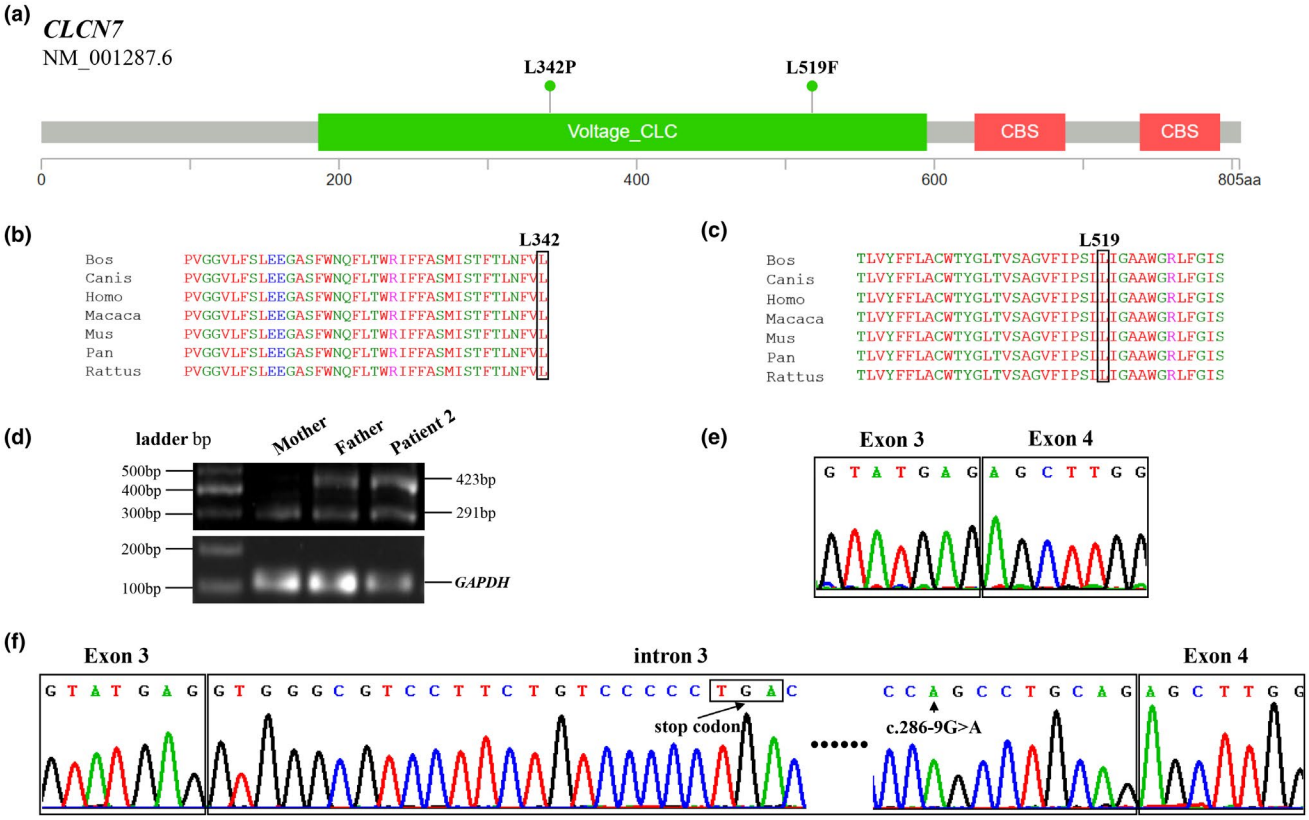

FIGURE 3 In silico and in vitro analysis of the three novel variants in the *CLCN7* gene. (a) The p.L342P and p.L519F variants are located in the voltage-gated chloride channel domain of the CLCN7 protein, which is a pfam domain. (b and c) A cross-species alignment of amino acid sequences showed that p.L342P and p.L519F variants occurred in a highly conserved region. (d) Electrophoresis of the RT-PCR products from the cDNA samples obtained from patient 2 and her father showed two *CLCN7* fragments of different sizes, whereas samples obtained from the patient's mother showed only one band. (e and f) Clone sequencing of RT-PCR products revealed that the c.286-9G>A variant leads to the retention of intron 3 and formation of a premature stop codon (p.E95Vfs*8), compared to the wild-type sequence

TABLE 2 Pathogenicity predictions of c.1025T>C (p.L342P) and c.1555C>T (p.L519F) in *CLCN7* gene

	c.1025T>C, p.L342P		c.1555C>T, p.L519F	
Prediction software	**Score**	**Prediction**	**Score**	**Prediction**
PolyPhen-2	1	Possibly damaging	1	Probably damaging
PROVEAN	−11.48	Deleterious	−11.59	Deleterious
Mutation Assessor	3.13	Medium (functional impact)	2.36	Medium (functional impact)
MutationTaster	1	Disease causing	1	Disease causing

displayed a normal splicing sequence (Figure 3e), whereas the c.286-9G>A variant generated a new "AG" splice receptor in intron 3, which led to aberrant splicing that retained intron 3 (Figure 3f). Further sequence analysis showed that this aberrant splicing resulted in the formation of a premature stop codon (p.E95Vfs*8).

3.4 | Treatment and follow-up

Five patients in this study were eventually diagnosed with ARO based on the genotype along with the clinical and laboratory data. Patients 1 and 2 were diagnosed with the *CLCN7*-dependent ARO, whereas patients 3B, 4, and 5 were diagnosed with the *TCIRG1*-dependent ARO. Considering the poor prognosis of transplantation for the patients with *CLCN7*-dependent ARO and neurodegeneration (Herebian et al., 2017; Shamriz et al., 2017), patient 1 and patient 2, with optic nerve symptoms, were withdrawn from the treatment. The three children with *TCIRG1* variants received allogeneic HSCT, and a re-examination in 1 year after the transplantation showed good recovery. The results of blood count, ALP level, and immunoglobulin levels returned to normal. The liver and spleen were

not palpable under the ribs. X-ray examination of Patient 5 in 1 and 2 years after transplantation showed that bone density decreased significantly (Figure S1a,b).

4 | DISCUSSION

In this study, we reported five osteopetrosis patients and identified two compound heterozygous variants in the *CLCN7* gene and three compound heterozygous variants in the *TCIRG1* gene. Among the variants, c.286-9G>A, c.1025T>C (p.L342P), and c.1555C>T (p.L519F) in *CLCN7*, and c.676G>T (p.E226*), c.1191del (p.P398Sfs*5), c.1370del (p.T457Tfs*71), and c.1554+2T>C in *TCIRG1* were novel. The splicing variant c.286-9G>A led to the retention of intron 3 in *CLCN7*, which resulted in the formation of a premature stop codon (p.E95Vfs*8). Two novel missense *CLCN7* variants, c.1025T>C (p.L342P) and c.1555C>T (p.L519F), occurred in the voltage-gated chloride channel domain, at the positions highly conserved in multiple species. Consistently, both variants were predicted to be deleterious by multiple *in silico* tools, indicating impaired function of the CLCN7 protein. In addition, sequence analysis showed that c.676G>T (p.E226*), c.1191del (p.P398Sfs*5), and c.1370del (p.T457Tfs*71) variants resulted in the loss of the partial peptide chain at the C-terminal domain of *TCIRG1*, leading to defects in the V-ATPase proton-pumping and vesicle trafficking functions in osteoclasts (Sobacchi et al., 2013). The c.1554+2T>C variant occurred in the splice donor site of intron 13, which was predicted to interfere with the splicing of exon 13 with exon 14 of *TCIRG1*. According to the guidelines issued by the American College of Medical Genetics and Genomics (Richards et al., 2015), all the variants were classified as pathogenic or likely pathogenic (Table S2).

The chloride channel family proteins are homodimers consisting of two homologous subunits, and each subunit has four Cl^- binding sites, eighteen intramembrane α helices, and two cystathionine beta synthase domains (Sui et al., 2013). The proteins of this family play an important role in both organelles and the plasma membrane, regulating ion homeostasis, cell volume, trans-epithelial transport, and electrical excitability (Faundez & Hartzell, 2004). As a member of this family, CLCN7 is a Cl^-/H^+ antiporter that mediates Cl^- conductance in osteoclast lysosomes, ensuring acidification necessary for bone degradation and resorption (Deng et al., 2016). Disruption of CLCN7 expression causes severe lysosomal storage disease, which in addition to osteopetrosis, leads to neurodegeneration, including retinal atrophy (Kasper et al., 2005). This suggests that neurological abnormalities in patients with *CLCN7*-dependent ARO may be caused by the dysregulation of lysosomal storage, in addition to the secondary effects caused by cranial stenosis compressing blood vessels and nerves that pass through it. To date, more than 100 variants of *CLCN7* have been included in the HGMD database (http://www.hgmd.cf.ac.uk/). Of them, several hotspots were described in patients of different ethnic origins, including c.296A>G (p.Y99C), c.643G>A (p.G215R), and c.2299C>T (p.R767W) (Letizia et al., 2004; Waguespack et al., 2003). The c.2299C>T (p.R767W) variant was first reported in Chinese ARO patient. Comparing the clinical characteristics of patients with ADO-II that harbor the same R767W variant in *CLCN7* gene, we found that the patients presented with varying disease severity, and some family members harboring the same heterozygous variant were normal, without any obvious clinical and radiographic abnormalities (Deng et al., 2016; Letizia et al., 2004; Li et al., 2019; Waguespack et al., 2003, 2007; Wang et al., 2012; Zhang et al., 2009; Zheng et al., 2016). It is still difficult to establish a robust correlation between the genotype and osteopetrosis phenotype in patients with *CLCN7* variants (Wang et al., 2012; Zheng et al., 2016). Patient 2 with compound heterozygous variants c.286-9G>A and c.1025T>C in *CLCN7* displayed a classic ARO phenotype. However, Zeng et al. (2016) reported a patient with a similar compound heterozygous variant, c.285+1G>A, and c.896C>T (p.A299V) in *CLCN7* that presented with distinct manifestations. That patient showed typical ARO phenotype at 7 months of age, but the clinical manifestations did not change significantly over the next 4 years, showing extremely slow disease progression (Zeng et al., 2016). Authors speculated that this difference was due to the patient's general genetic background, suggesting that certain “compensatory” or “modifier” mechanisms in the acidification system “buffered” the disease progression. It has been reported that the variable phenotype in patients with *CLCN7* gene variants may be explained by the activity of the modifier genes (Rivas et al., 2015). Although several studies have suggested the presence of modifier genes affecting the course of *CLCN7*-dependent osteopetrosis, the mechanism through which *CLCN7* gene defects cause osteopetrosis is extremely complicated, and the relationship between the genotype and phenotype is still unclear. Further studies involving a larger cohort of patients with osteopetrosis and healthy individuals who carry *CLCN7* gene mutations will be useful in providing information to determine this mechanism.

The main function of the V-ATPase proton pump is to maintain an acidic microenvironment between osteoclasts and bone tissue to promote bone resorption (Ajmal et al., 2017). The V-ATPase proton pump is a multi-subunit membrane complex with two main domains: the transmembrane proton translocation domain V0 promotes extracellular acidification of organelles and the cytosolic hydrolytic domain V1 mediates ATP hydrolysis (Anderson

et al., 2015). Defects in different subunits of the V-ATPase protein complex are thought to be responsible for osteopetrosis (Stark et al., 2013). Variants of *TCIRG1*, which encodes the a3 subunit of the V-ATPase complex, are reportedly most frequently associated with ARO. So far, nearly 100 variants of *TCIRG1* have been found in patients with ARO (HGMD database). Several variants (c.807+5G>A, c.1213G>A, c.2005C>T, c.1674-1G>A, and others) have been reported at higher frequencies in well-defined Costa Rican, Chuvashian, and Belgian populations, owing to the founder effect, long reproductive isolation, and genetic drift (Bliznetz et al., 2009; Pangrazio, Caldana, et al., 2012; Sobacchi et al., 2001; Susani et al., 2004). Clinical data show that patients with ARO and *TCIRG1* variants generally present with a homogeneous phenotype that includes prominent bone defects, secondary hematological and neurological impairment, rare major immunological deficits, and they respond well to HSCT (Mazzolari et al., 2009; Pangrazio, Caldana, et al., 2012; Villa et al., 2009). Three patients with ARO and *TCIRG1* variants in this study showed this typical malignant phenotype. A small subset of patients with specific molecular defects displayed a different phenotype. Sobacchi et al. (2014) and Zhang et al. (2017) reported mild forms of *TCIRG1*-dependent ARO in several patients. A common feature in these patients was that a single-nucleotide change in the middle of an intron led to an incomplete splicing, which retained a small amount of normal TCIRG1 protein (Palagano et al., 2015; Sobacchi et al., 2014; Zhang et al., 2017). Sobacchi et al. (2014) demonstrated that even a limited amount of normal TCIRG1 protein was sufficient to dampen the clinical outcomes. This finding may provide a new treatment direction, in addition to HSCT, for osteopetrosis patients with *TCIRG1* variants.

To the best of our knowledge, the positive effects of HSCT on intrinsic osteoclast abnormalities, abnormal bone metabolism, and extramedullary hematopoiesis are more pronounced in patients with ARO that harbor *TCIRG1* variants (Kuroyanagi et al., 2014). However, many complications have been reported in patients with ARO after HSCT (Kuroyanagi et al., 2014). In this study, three patients received Allo-HSCT treatment, and although their bone density was reduced and bone marrow hematopoiesis recovered, the effects required a longer follow-up period to draw definitive conclusions. The latest research shows that the resorptive function of human ARO osteoclasts can be restored in vitro by lentiviral vector-mediated expression of TCIRG1 in $CD34^+$ cells of patients with ARO and *TCIRG1* variants, followed by the differentiation into mature osteoclasts (Moscatelli et al., 2021; Thudium et al., 2016). Capo et al. (2021) demonstrated that the small molecule pyrimidoindole derivative UM171 stimulated the expansion of hematopoietic stem and progenitor cells in vitro and enhanced lentiviral transduction efficiency without affecting their long-term repopulating potential and ability to generate functional osteoclasts. Autologous corrected stem cells transplantation represents a potentially safe and promising therapeutic alternative for patients with ARO, as it does not require suitable allogeneic donors and can restore the function of osteoclasts without some transplant-related complications, such as graft-versus-host disease (Moscatelli et al., 2021; Xian et al., 2020).

The clinical features and laboratory findings in patients with ARO and those with JMML may be similar. Patients with ARO and JMML may present with anemia, leukocytosis, monocytosis, thrombocytopenia, granulocytopenia, and hepatosplenomegaly (Hoyoux et al., 2014). This may be the reason why Patient 3A was misdiagnosed with JMML. Although both diseases can be treated with HSCT, the indications and preparative regimens for HSCT differ (Strauss et al., 2015). Therefore, careful differential diagnosis is essential between ARO and JMML. Elevation of ALP, hypoglobulinemia, and increased bone density are not described in patients with JMML (Hoyoux et al., 2014; Strauss et al., 2015). Imaging examination showed that increased bone density is an effective diagnostic method for distinguishing between these two diseases. Using high-throughput sequencing technology to find specific genetic molecular markers enabling precise molecular diagnosis is the most powerful and accurate way to distinguish these two diseases.

In summary, five Chinese children suspected to have osteopetrosis were studied and eventually diagnosed with ARO based on clinical manifestations, biochemical examination, radiological changes, and genetic defects. Seven novel variants, c.286-9G>A, c.1025T>C (p.L342P), and c.1555C>T (p.L519F) in *CLCN7* as well as c.676G>T (p.E226*), c.1191del (p.P398Sfs*5), c.1370del (p.T457Tfs*71), and c.1554+2T>C in *TCIRG1* were identified in these patients. This report not only expands the variation spectrum of the *TCRIG1* and *CLCN7* genes, but also deepens our understanding of the relationship between genotype and clinical characteristics of osteopetrosis.

ACKNOWLEDGMENTS

The authors thank all the patients and their parents for participation in this study. This research was sponsored by grants from the Program of Shanghai Academic/Technology Research Leader (19XD1422600 and 2018BR28), Project of Shanghai Municipal Science and Technology Commission (20dz2260900), and Shuguang Program supported by the Shanghai Education Development Foundation and Shanghai Municipal Education Commission (18SG14).

CONFLICT OF INTEREST

The authors have declared no conflict of interest.

AUTHOR CONTRIBUTIONS

Huanhuan Liang: Writing - original draft, investigation, visualization, and conceptualization. Niu Li: Writing - original draft and investigation. Ru-en Yao: Writing - review and editing. Tingting Yu: Resources, writing- review and editing. Lixia Ding: Resources, writing- review and editing. Jing Chen: Data curation, conceptualization, and supervision. Jian Wang: Data curation, conceptualization, supervision, and funding acquisition.

ETHICAL APPROVAL

All procedures were performed in accordance with the ethical standards of the responsible institutional committee on human experimentation and with the Helsinki Declaration of 1975, as revised in 2000. The protocol was approved by the Ethics Committee of the Shanghai Children's Medical Center (SCMCIRB-K2016013).

DATA AVAILABILITY STATEMENT

The data that support the findings of this study are available on request from the corresponding authors.

ORCID

Huanhuan Liang https://orcid.org/0000-0002-1803-3121
Niu Li https://orcid.org/0000-0001-6504-7633
Ru-en Yao https://orcid.org/0000-0003-4147-5291

REFERENCES

Ajmal, M., Mir, A., Wahid, S., Khor, C. C., Foo, J. N., Siddiqi, S., Kauser, M., Malik, S. A., & Nasir, M. (2017). Identification and in silico characterization of a novel p.P208PfsX1 mutation in V-ATPase a3 subunit associated with autosomal recessive osteopetrosis in a Pakistani family. *BMC Medical Genetics*, *18*(1), 148. https://doi.org/10.1186/s12881-017-0506-4

Anderson, S. L., Jalas, C., Fedick, A., Reid, K. F., Carpenter, T. O., Chirnomas, D., & Rubin, B. Y. (2015). A founder mutation in the TCIRG1 gene causes osteopetrosis in the Ashkenazi Jewish population. *Clinical Genetics*, *88*(1), 74–79. https://doi.org/10.1111/cge.12448

Besbas, N., Draaken, M., Ludwig, M., Deren, O., Orhan, D., Bilginer, Y., & Ozaltin, F. (2009). A novel CLCN7 mutation resulting in a most severe form of autosomal recessive osteopetrosis. *European Journal of Pediatrics*, *168*(12), 1449–1454. https://doi.org/10.1007/s00431-009-0945-9

Bliznetz, E. A., Tverskaya, S. M., Zinchenko, R. A., Abrukova, A. V., Savaskina, E. N., Nikulin, M. V., Kirillov, A. G., Ginter, E. K., & Polyakov, A. V. (2009). Genetic analysis of autosomal recessive osteopetrosis in Chuvashiya: The unique splice site mutation in TCIRG1 gene spread by the founder effect. *European Journal of Human Genetics*, *17*(5), 664–672. https://doi.org/10.1038/ejhg.2008.234

Bonapace, G., Moricca, M. T., Talarico, V., Graziano, F., Pensabene, L., & Miniero, R. (2014). Identification of two novel mutations on CLCN7 gene in a patient with malignant ostopetrosis. *Italian Journal of Pediatrics*, *40*, 90. https://doi.org/10.1186/s13052-014-0090-6

Capo, V., Penna, S., Merelli, I., Barcella, M., Scala, S., Basso-Ricci, L., Draghici, E., Palagano, E., Zonari, E., Desantis, G., Uva, P., Cusano, R., Sergi Sergi, L., Crisafulli, L., Moshous, D., Stepensky, P., Drabko, K., Kaya, Z., Unal, E., ... Villa, A. (2021). Expanded circulating hematopoietic stem/progenitor cells as novel cell source for the treatment of TCIRG1 osteopetrosis. *Haematologica*, *106*(1), 74–86. https://doi.org/10.3324/haematol.2019.238261

Deng, H., He, D., Rong, P., Xu, H., Yuan, L., Li, L., Lu, Q., & Guo, Y. (2016). Novel CLCN7 mutation identified in a Han Chinese family with autosomal dominant osteopetrosis-2. *Molecular Pain*, *12*(7), 1–7. https://doi.org/10.1177/1744806916652628

Faundez, V., & Hartzell, H. C. (2004). Intracellular chloride channels: Determinants of function in the endosomal pathway. *Science Signaling*, *2004*(233), re8. https://doi.org/10.1126/stke.2332004re8

Herebian, D., Alhaddad, B., Seibt, A., Schwarzmayr, T., Danhauser, K., Klee, D., Harmsen, S., Meitinger, T., Strom, T. M., Schulz, A., Mayatepek, E., Haack, T. B., & Distelmaier, F. (2017). Coexisting variants in OSTM1 and MANEAL cause a complex neurodegenerative disorder with NBIA-like brain abnormalities. *European Journal of Human Genetics*, *25*(9), 1092–1095. https://doi.org/10.1038/ejhg.2017.96

Hoyoux, C., Dresse, M. F., Forget, P., Piette, C., Rausin, L., Villa, A., Gothot, A., & Florkin, B. (2014). Osteopetrosis mimicking juvenile myelomonocytic leukemia. *Pediatrics International*, *56*(5), 779–782. https://doi.org/10.1111/ped.12342

Kasper, D., Planells-Cases, R., Fuhrmann, J. C., Scheel, O., Zeitz, O., Ruether, K., Schmitt, A., Poët, M., Steinfeld, R., Schweizer, M., Kornak, U., & Jentsch, T. J. (2005). Loss of the chloride channel ClC-7 leads to lysosomal storage disease and neurodegeneration. *EMBO Journal*, *24*(5), 1079–1091. https://doi.org/10.1038/sj.emboj.7600576

Kuroyanagi, Y., Kawasaki, H., Noda, Y., Ohmachi, T., Sekiya, S.-I., Yoshimura, K., Ohe, C., Michigami, T., Ozono, K., & Kaneko, K. (2014). A fatal case of infantile malignant osteopetrosis complicated by pulmonary arterial hypertension after hematopoietic stem cell transplantation. *Tohoku Journal of Experimental Medicine*, *234*(4), 309–312. https://doi.org/10.1620/tjem.234.309

Letizia, C., Taranta, A., Migliaccio, S., Caliumi, C., Diacinti, D., Delfini, E., D'Erasmo, E., Iacobini, M., Roggini, M., Albagha, O. M., Ralston, S. H., & Teti, A. (2004). Type II benign osteopetrosis (Albers-Schonberg disease) caused by a novel mutation in CLCN7 presenting with unusual clinical manifestations. *Calcified Tissue International*, *74*(1), 42–46. https://doi.org/10.1007/s00223-002-1087-5

Li, L., Lv, S. S., Wang, C., Yue, H., & Zhang, Z. L. (2019). Novel CLCN7 mutations cause autosomal dominant osteopetrosis type II and intermediate autosomal recessive osteopetrosis. *Molecular Medicine Reports*, *19*(6), 5030–5038. https://doi.org/10.3892/mmr.2019.10123

Li, Y. P., Chen, W., Liang, Y., Li, E., & Stashenko, P. (1999). Atp6i-deficient mice exhibit severe osteopetrosis due to loss of osteoclast-mediated extracellular acidification. *Nature Genetics*, *23*(4), 447–451. https://doi.org/10.1038/70563

Mazzolari, E., Forino, C., Razza, A., Porta, F., Villa, A., & Notarangelo, L. D. (2009). A single-center experience in 20 patients with infantile malignant osteopetrosis. *American Journal of Hematology*, *84*(8), 473–479. https://doi.org/10.1002/ajh.21447

Moore, J. B., Hoang, T. D., & Shwayhat, A. F. (2017). Case report of clinical vignette: Osteopetrosis. *Military Medicine*, *182*(3), e1886–e1888. https://doi.org/10.7205/MILMED-D-16-00234

Moscatelli, I., Almarza, E., Schambach, A., Ricks, D., Schulz, A., Herzog, C. D., Henriksen, K., Askmyr, M., Schwartz, J. D., & Richter, J. (2021). Gene therapy for infantile malignant osteopetrosis: Review of pre-clinical research and proof-of-concept for phenotypic reversal. *Molecular Therapy - Methods & Clinical Development*, *20*, 389–397. https://doi.org/10.1016/j.omtm.2020.12.009

Palagano, E., Blair, H. C., Pangrazio, A., Tourkova, I., Strina, D., Angius, A., Cuccuru, G., Oppo, M., Uva, p., Van Hui, W., Boudin, E., Superti-Furga, A., Faletra, F., Nocerino, A., Ferrari, M.C., Grappiolo, G., Monari, M., Montanelli, A., Vezzoni, P., ... Sobacchi, C. (2015). Buried in the Middle but Guilty: Intronic mutations in the TCIRG1 gene cause human autosomal recessive osteopetrosis. *Journal of Bone and Mineral Research*, *30*(10), 1814–1821. https://doi.org/10.1002/jbmr.2517

Pangrazio, A., Caldana, M. E., Lo Iacono, N., Mantero, S., Vezzoni, P., Villa, A., & Sobacchi, C. (2012). Autosomal recessive osteopetrosis: Report of 41 novel mutations in the TCIRG1 gene and diagnostic implications. *Osteoporosis International*, *23*(11), 2713–2718. https://doi.org/10.1007/s00198-011-1878-5

Pangrazio, A., Frattini, A., Valli, R., Maserati, E., Susani, L., Vezzoni, P., Villa, A., Al-Herz, W., & Sobacchi, C. (2012). A homozygous contiguous gene deletion in chromosome 16p13.3 leads to autosomal recessive osteopetrosis in a Jordanian patient. *Calcified Tissue International*, *91*(4), 250–254. https://doi.org/10.1007/s00223-012-9631-4

Pangrazio, A., Puddu, A., Oppo, M., Valentini, M., Zammataro, L., Vellodi, A., Gener, B., Llano-Rivas, I., Raza, J., Atta, I., Vezzoni, P., Superti-Furga, A., Villa, A., & Sobacchi, C. (2014). Exome sequencing identifies CTSK mutations in patients originally diagnosed as intermediate osteopetrosis. *Bone*, *59*, 122–126. https://doi.org/10.1016/j.bone.2013.11.014

Richards, S., Aziz, N., Bale, S., Bick, D., Das, S., Gastier-Foster, J., Grody, W. W., Hegde, M., Lyon, E., Spector, E., Voelkerding, K., & Rehm, H. L. (2015). Standards and guidelines for the interpretation of sequence variants: A joint consensus recommendation of the American College of Medical Genetics and Genomics and the Association for Molecular Pathology. *Genetics in Medicine*, *17*(5), 405–424. https://doi.org/10.1038/gim.2015.30

Rivas, M. A., Pirinen, M., Conrad, D. F., Lek, M., Tsang, E. K., Karczewski, K. J., Maller, J. B., Kukurba, K. R., DeLuca, D. S., Fromer, M., Ferreira, P. G., Smith, K. S., Zhang, R., Zhao, F., Banks, E., Poplin, R., Ruderfer, D. M., Purcell, S. M., Tukiainen, T., ... Estivill, X. (2015). Human genomics. Effect of predicted protein-truncating genetic variants on the human transcriptome. *Science*, *348*(6235), 666–669. https://doi.org/10.1126/science.1261877

Shamriz, O., Shaag, A., Yaacov, B., NaserEddin, A., Weintraub, M., Elpeleg, O., & Stepensky, P. (2017). The use of whole exome sequencing for the diagnosis of autosomal recessive malignant infantile osteopetrosis. *Clinical Genetics*, *92*(1), 80–85. https://doi.org/10.1111/cge.12804

Sobacchi, C., Frattini, A., Orchard, P., Porras, O., Tezcan, I., Andolina, M., & Villa, A. (2001). The mutational spectrum of human malignant autosomal recessive osteopetrosis. *Human Molecular Genetics*, *10*(17), 1767–1773. https://doi.org/10.1093/hmg/10.17.1767

Sobacchi, C., Pangrazio, A., Lopez, A. G., Gomez, D. P., Caldana, M. E., Susani, L., Vezzoni, P., & Villa, A. (2014). As little as needed: The extraordinary case of a mild recessive osteopetrosis owing to a novel splicing hypomorphic mutation in the TCIRG1 gene. *Journal of Bone and Mineral Research*, *29*(7), 1646–1650. https://doi.org/10.1002/jbmr.2203

Sobacchi, C., Schulz, A., Coxon, F. P., Villa, A., & Helfrich, M. H. (2013). Osteopetrosis: Genetics, treatment and new insights into osteoclast function. *Nature Reviews Endocrinology*, *9*(9), 522–536. https://doi.org/10.1038/nrendo.2013.137

Stark, Z., Pangrazio, A., McGillivray, G., & Fink, A. M. (2013). Association of severe autosomal recessive osteopetrosis and structural brain abnormalities: A case report and review of the literature. *European Journal of Medical Genetics*, *56*(1), 36–38. https://doi.org/10.1016/j.ejmg.2012.10.001

Strauss, A., Furlan, I., Steinmann, S., Buchholz, B., Kremens, B., Rossig, C., Corbacioglu, S., Rajagopal, R., Lahr, G., Yoshimi, A., Strahm, B., Niemeyer, C. M., & Schulz, A. (2015). Unmistakable Morphology? Infantile Malignant Osteopetrosis Resembling Juvenile Myelomonocytic Leukemia in Infants. *Journal of Pediatrics*, *167*(2), 486–488. https://doi.org/10.1016/j.jpeds.2015.04.064

Sui, W., Ou, M., Liang, J., Ding, M., Chen, J., Liu, W., Xiao, R., Meng, X., Wang, L., Pan, X., Zhu, P., Xue, W., Zhang, Y., Lin, H., Li, F., Zhang, J., & Dai, Y. (2013). Rapid gene identification in a Chinese osteopetrosis family by whole exome sequencing. *Gene*, *516*(2), 311–315. https://doi.org/10.1016/j.gene.2012.12.072

Susani, L., Pangrazio, A., Sobacchi, C., Taranta, A., Mortier, G., Savarirayan, R., Villa, A., Orchard, P., Vezzoni, P., Albertini, A., Frattini, A., & Pagani, F. (2004). TCIRG1-dependent recessive osteopetrosis: Mutation analysis, functional identification of the splicing defects, and in vitro rescue by U1 snRNA. *Human Mutation*, *24*(3), 225–235. https://doi.org/10.1002/humu.20076

Thudium, C. S., Moscatelli, I., Löfvall, H., Kertész, Z., Montano, C., Bjurström, C. F., Karsdal, M. A., Schulz, A., Richter, J., & Henriksen, K. (2016). Regulation and function of lentiviral vector-mediated TCIRG1 expression in osteoclasts from patients with infantile malignant osteopetrosis: Implications for gene therapy. *Calcified Tissue International*, *99*(6), 638–648. https://doi.org/10.1007/s00223-016-0187-6

Villa, A., Guerrini, M. M., Cassani, B., Pangrazio, A., & Sobacchi, C. (2009). Infantile malignant, autosomal recessive osteopetrosis: The rich and the poor. *Calcified Tissue International*, *84*(1), 1–12. https://doi.org/10.1007/s00223-008-9196-4

Waguespack, S. G., Hui, S. L., Dimeglio, L. A., & Econs, M. J. (2007). Autosomal dominant osteopetrosis: Clinical severity and natural history of 94 subjects with a chloride channel 7 gene mutation. *Journal of Clinical Endocrinology and Metabolism*, *92*(3), 771–778. https://doi.org/10.1210/jc.2006-1986

Waguespack, S. G., Koller, D. L., White, K. E., Fishburn, T., Carn, G., Buckwalter, K. A., Johnson, M., Kocisko, M., Evans, W. E., Foroud, T., & Econs, M. J. (2003). Chloride channel 7 (ClCN7) gene mutations and autosomal dominant osteopetrosis, type II. *Journal of Bone and Mineral Research*, *18*(8), 1513–1518. https://doi.org/10.1359/jbmr.2003.18.8.1513

Wang, C., Zhang, H., He, J.-W., Gu, J.-M., Hu, W.-W., Hu, Y.-Q., Li, M., Liu, Y.-J., Fu, W.-Z., Yue, H., Ke, Y.-H., & Zhang, Z.-L. (2012). The virulence gene and clinical phenotypes of osteopetrosis in the Chinese population: Six novel mutations of the CLCN7 gene in twelve osteopetrosis families. *Journal of Bone and Mineral Metabolism*, *30*(3), 338–348. https://doi.org/10.1007/s00774-011-0319-z

Xian, X., Moraghebi, R., Löfvall, H., Fasth, A., Henriksen, K., Richter, J., Woods, N.-B., & Moscatelli, I. (2020). Generation of gene-corrected functional osteoclasts from osteopetrotic induced pluripotent stem cells. *Stem Cell Research & Therapy*, *11*(1), 179. https://doi.org/10.1186/s13287-020-01701-y

Yu, T., Yu, Y., Wang, J., Yin, L., Zhou, Y., Ying, D., Huang, R., Chen, H., Wu, S., Shen, Y., Fu, Q., & Chen, F. (2014). Identification of TCIRG1 and CLCN7 gene mutations in a patient with autosomal recessive osteopetrosis. *Molecular Medicine Reports*, *9*(4), 1191–1196. https://doi.org/10.3892/mmr.2014.1955

Zeng, B., Li, R. U., Hu, Y., Hu, B., Zhao, Q., Liu, H., Yuan, P., & Wang, Y. (2016). A novel mutation and a known mutation in the CLCN7 gene associated with relatively stable infantile malignant osteopetrosis in a Chinese patient. *Gene*, *576*(1 Pt 1), 176–181. https://doi.org/10.1016/j.gene.2015.10.021

Zhang, X. Y., He, J. W., Fu, W. Z., Wang, C., & Zhang, Z. L. (2017). Novel mutations of TCIRG1 cause a malignant and mild phenotype of autosomal recessive osteopetrosis (ARO) in four Chinese families. *Acta Pharmacologica Sinica*, *38*(11), 1456–1465. https://doi.org/10.1038/aps.2017.108

Zhang, Z.-L., He, J.-W., Zhang, H., Hu, W.-W., Fu, W.-Z., Gu, J.-M., Yu, J.-B., Gao, G., Hu, Y.-Q., Li, M., & Liu, Y.-J. (2009). Identification of the CLCN7 gene mutations in two Chinese families with autosomal dominant osteopetrosis (type II). *Journal of Bone and Mineral Metabolism*, *27*(4), 444–451. https://doi.org/10.1007/s00774-009-0051-0

Zheng, H., Shao, C., Zheng, Y., He, J. W., Fu, W. Z., Wang, C., & Zhang, Z. L. (2016). Two novel mutations of CLCN7 gene in Chinese families with autosomal dominant osteopetrosis (type II). *Journal of Bone and Mineral Metabolism*, *34*(4), 440–446. https://doi.org/10.1007/s00774-015-0682-2

SUPPORTING INFORMATION

Additional Supporting Information may be found in the online version of the article at the publisher's website.

How to cite this article: Liang, H., Li, N., Yao, R.-E., Yu, T., Ding, L., Chen, J., & Wang, J. (2021). Clinical and molecular characterization of five Chinese patients with autosomal recessive osteopetrosis. *Molecular Genetics & Genomic Medicine*, 9, e1815. https://doi.org/10.1002/mgg3.1815